



Measuring the Neutrino Magnetic Moment in the NOvA Near Detector

Róbert Králik

Supervisor: Dr. Lily Asquith

*A thesis submitted in fulfilment of the requirements for the degree of
Doctor of Philosophy to the*

School of Mathematical and Physical Sciences
University of Sussex

In Brighton, United Kingdom

February 28, 2024

I hereby declare that I carried out this thesis independently, and only with the cited sources, literature and other professional sources.

I also declare that this thesis has not been and will not be, submitted in whole or in part to another University for the award of any other degree.

Brighton, United Kingdom,

February 28, 2024

Róbert Králik

Acknowledgements

School of Mathematical and Physical Sciences, University of Sussex

DOCTORAL THESIS

Measuring the Neutrino Magnetic Moment in the NOvA Near
Detector

by Róbert Králik

ABSTRACT

Abstract

Keywords:

Contents

| | |
|--|-----------|
| Acknowledgements | ii |
| List of Figures | v |
| List of Tables | vi |
| 1 The NOvA experiment | 1 |
| 1.1 The Neutrino Beam | 1 |
| 1.2 The NOvA Detectors | 4 |
| 1.3 Data Acquisition | 6 |
| 1.4 Data Processing and Event Reconstruction | 8 |
| 1.5 Simulation | 8 |
| 1.5.1 Neutrino Beam Simulation | 8 |
| 1.5.2 Simulation of the Neutrino Interactions | 9 |
| 1.5.3 Simulation of the Detector Response | 9 |
| 1.6 Detector Calibration | 9 |
| 1.6.1 Threshold and shielding correction | 13 |
| 1.6.2 Relative calibration | 13 |
| 1.6.3 Absolute calibration | 15 |
| 1.7 Systematic Uncertainties at NOvA | 15 |
| 1.7.1 Systematic Uncertainties Related to the NOvA Neutrino Beam | 15 |
| 1.7.2 Systematic uncertainties for NOvA detectors | 16 |
| Glossary | 17 |
| Bibliography | 18 |

List of Figures

| | | |
|-----|--|----|
| 1.1 | The schematic of the NuMI beam facility | 2 |
| 1.2 | NuMI neutrino beam components in the NOvA near detector | 3 |
| 1.3 | The NOvA off-axis beam concept | 3 |
| 1.4 | NOvA detectors | 4 |
| 1.5 | NOvA Avalanche Photo Diodes | 6 |
| 1.6 | NOvA Front End Board | 7 |
| 1.7 | Illustration of the tricell condition (a). We only use hits that have two surrounding hits in the same plane to be used in the NOvA calibration. This is to ensure a good quality of the path length (d) reconstruction, which is calculated from the known cell height (h) and the reconstructed track angle (φ). In case the hit is next to a bad channel (b), we ignore this bad channel and require a hit in the next cell over. | 10 |
| 1.8 | The Test Beam detector is (like the standard NOvA detectors) divided into 12 brightness bins (left plot), each representing a relative difference in energy response (right plot) due to different brightnesses of the fibres, scintillators, or readout. | 11 |

List of Tables

| | |
|---|----|
| 1.1 Definitions of variables commonly used in calibration [? ?]. | 12 |
|---|----|

CHAPTER 1

The NOvA experiment

The NuMI Off-axis ν_e Appearance (NOvA) experiment [1] is a long-baseline neutrino oscillation experiment based at the Fermi National Accelerator Laboratory (Fermilab) [2]. NOvA receives an off-axis ν_μ and $\bar{\nu}_\mu$ beam from Fermilab's NuMI neutrino source, described in Sec. 1.1, and measures $\nu_e/\bar{\nu}_e$ appearance and $\nu_\mu/\bar{\nu}_\mu$ disappearance between its two highly active and finely segmented detectors, described in Sec. 1.4 [3].

The capability to measure both ν_e and $\bar{\nu}_e$ appearance, coupled with a significant matter effect induced by the long baseline, allows NOvA to address some of the most important questions in neutrino physics to date, such as the neutrino mass ordering, the octant of θ_{23} , and the possible CP violation in the neutrino sector [3–7]. NOvA also measures the values of θ_{13} , θ_{23} and $|\Delta m_{atm}^2|$ [3], but also measures neutrino differential cross sections in the near detector [8–11], provides constraint on the possible sterile neutrino models [12, 13], monitors for supernova neutrino activity [14, 15], searches for magnetic monopoles [16], or constrains neutrino electromagnetic properties (this thesis) amongst other topics. Using two functionally identical detectors mitigates the systematic uncertainties of neutrino oscillation measurements, described in Sec. 1.7.

COMMENT: *Should I mention here when did NOvA start taking data and how long is it planning to run for? Maybe future analysis? Size of the collaboration?* - YES!

1.1 The Neutrino Beam

The neutrino beam for NOvA comes from the Fermilab-based *Neutrinos at the Main Injector* (NuMI) neutrino source [17]. The schematic description of NuMI is shown on Fig. 1.1, starting on the left hand side with 120 GeV protons from the Main Injector, part of the Fermilab accelerator complex. The proton beam is divided into 10 μs long

pulses, with $\sim 5 \times 10^{13}$ protons on target (POT) per spill every ~ 1.3 s long cycle time, resulting in a proton beam power of ~ 800 kW, with upgrades currently underway to surpass 1 MW [18].

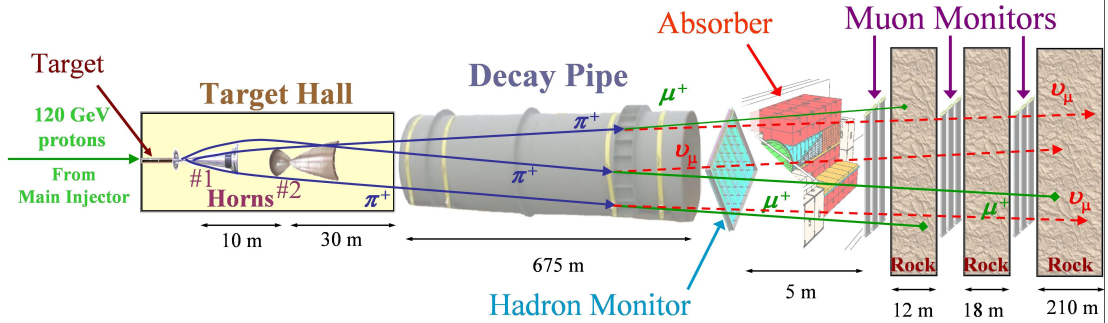


Figure 1.1: The NuMI neutrino beam starts on the left hand side with protons from the Main Injector impinged on a graphite target producing mainly pions and kaons. These are then focused and charge-selected by two focusing horns, after which they decay inside the decay pipe into a high-purity muon neutrino, or antineutrino beam. The residual hadrons are stopped and monitored in the hadron absorber and the remaining muons are recorded with muon monitors and absorbed inside the rock.

The proton beam passes through a collimating baffle before hitting a ~ 1.2 m-long graphite target [19], producing hadrons, predominantly pions and kaons [17]. These are then focused and selected by two parabolic magnetic "horns". Using a positive current inside the horns focuses positively charged particles, which then decay into neutrinos, and removes negatively charged particles. Reversing the horn current on the other hand focuses negatively charged particles, which decay into antineutrinos, and defocuses positively charged particles. The neutrino mode is therefore called Forward Horn Current (FHC) and the antineutrino mode is called Reverse Horn Current (RHC). The composition of the neutrino beam for both these modes at the NOvA near detector, shown as a rate of charge current events, is presented on Fig. 1.2, displaying the very high purity of ν_μ component in the FHC beam, and the high purity of $\bar{\nu}_\mu$ component in the RHC mode [17].

The focused hadrons pass through a 675 m-long decay pipe filled with helium to create a low density environment for hadrons to propagate and decay into neutrinos, or antineutrinos [17, 19]. High energy hadrons that do not decay in the decay pipe are absorbed within a massive aluminium, steel and concrete hadron absorber and monitored with a hadron monitor [17]. The leftover muons are ranged out in a dolomite rock after the absorber and monitored using three muon monitors. The hadron and

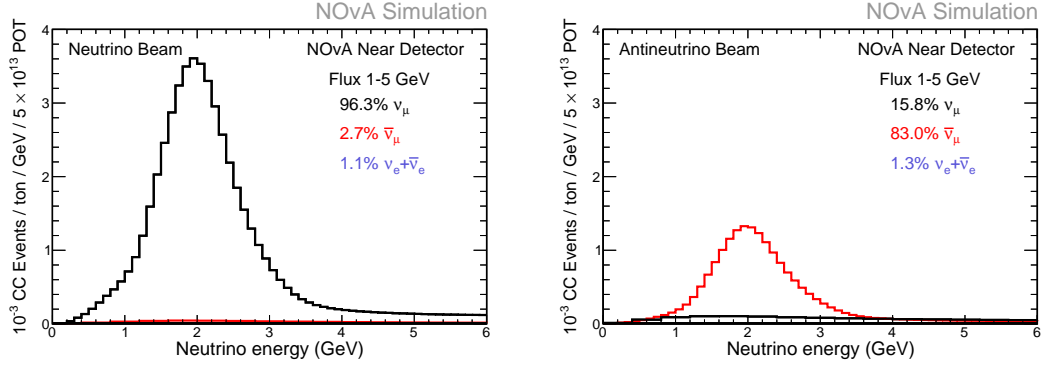


Figure 1.2: The charge current event rates for different neutrino flavours, as measured at the NOvA Near Detector in the FHC regime shown on the left, or the RHC regime on the right. The contribution of neutrino flavours to the event rates is also displayed, showing the high purity of the neutrino beam for NOvA.

all the muon monitors are ionization chambers, used to monitor the quality, location and relative intensity of the beam [17].

The resulting neutrino beam is peaked ~ 7 GeV with a wide energy band. However, thanks to the kinematics of the dominant pion decay, by placing NOvA detector 14.6 mrad ($\approx 0.8^\circ$) off the main NuMI beam axis, we achieve a narrow band neutrino flux peaked at 1.8 GeV [7, 20], as can be seen on Fig. 1.3. Using an off-axis neutrino flux increases the neutrino beam around 2 GeV about 5-fold compared to the on-axis flux and enhances background rejection for the ν_e appearance analysis [20].

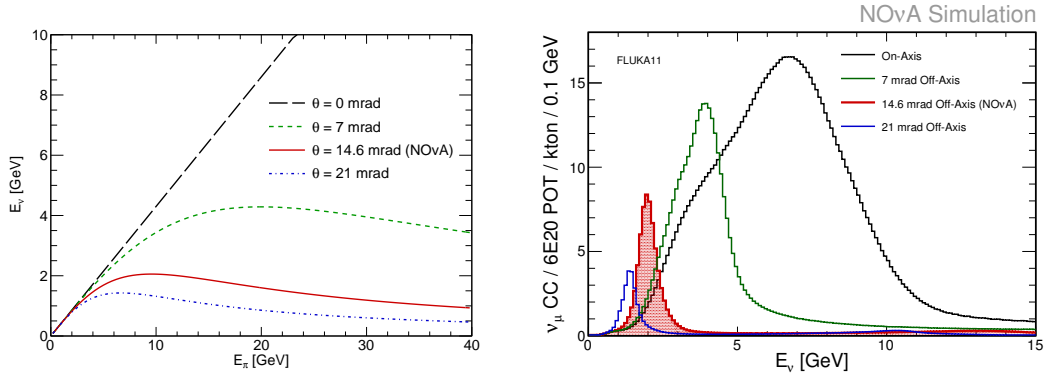


Figure 1.3: Dependence of the neutrino energy on the parent pion's energy and a neutrino energy distribution for an on-axis beam and three different off-axis beam designs. The case for NOvA is shown here in red and results in a narrow neutrino energy distribution around 2 GeV, independent on the parent pion's energy.

1.2 The NOvA Detectors

COMMENT: Lot of this information is just from the TDR, only rarely from other sources. I don't want to reference the TDR after every information/sentence. Should I just put the reference somewhere into each paragraph (like it is now), or would it be enough to reference it less, assuming the reader will figure out where does most of this info come from?

The two main NOvA detectors are the Near Detector (ND), located in Fermilab ~ 1 km from the NuMI target and ~ 100 m under ground, and the Far Detector (FD), located ~ 810 km from Fermilab at Ash River in north Minnesota, partially underground with a rock overburden [20]. NOvA also operated a detector prototype called Near Detector on the Surface (NDOS) used for an early research and development of detector components and analysis [4]. Additionally, NOvA operated a NOvA Test Beam detector (TB), described in detail in Sec. ???. The scale of the near and far detectors are shown on Fig. 1.4.

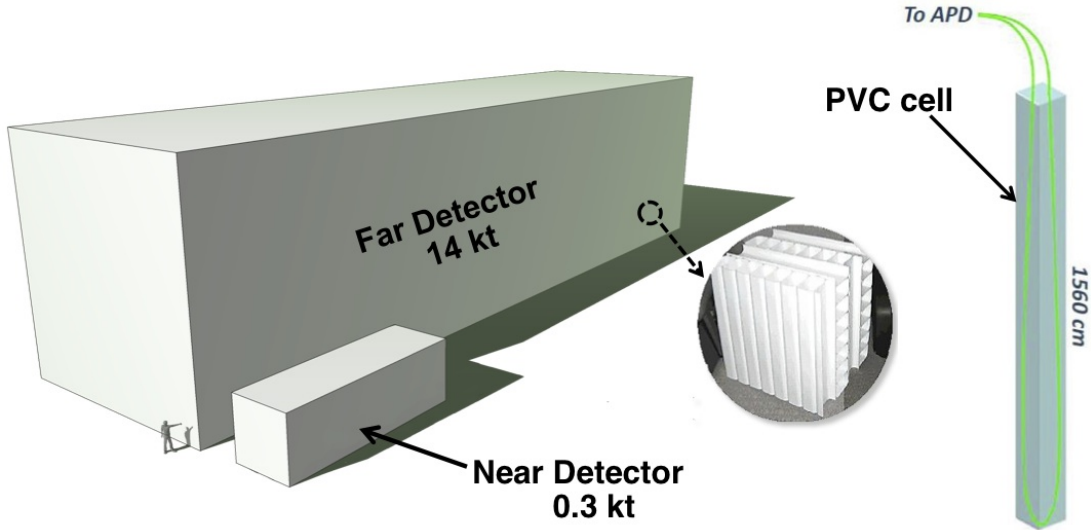


Figure 1.4: Schematic description of scale and composition of the NOvA detectors. Inset is showing a photo of the orthogonal planes made out of PVC cells. An example of a far detector cell containing liquid scintillator and a loop of wavelength sifting fibre attached to an avalanche photodiode is shown on the right [21].

All NOvA detectors are highly segmented, highly active, functionally identical tracking calorimeters made up of polyvinyl chloride (PVC) cells filled with liquid scintillator. Each cell is a cuboid with depth of 5.9 cm (along the depth of the detector) and width of 3.8 cm (with some variations), with cell length extending to the

full width/height of each detector, which is ≈ 4 m for the ND and ≈ 15 m for the FD [20]. An example of a FD cell is shown on the right of Fig. 1.4.

Cells are connected side-by-side into a 16 cell-wide extrusions with 3.3 mm-wide walls between cells and 4.9 mm-wide walls on the outsides of the extrusions. The first and last cell of each extrusion are ~ 3 mm narrower than the rest of the cells. Two extrusions are connected side-by-side to form a 32 cell-wide module, with each module having a separate readout (see Sec. 1.3). In the FD, 12 modules are connected side-by-side to form one plane of the detector. In the ND only 3 modules make up a plane. Planes are positioned one after another, alternating between vertical and horizontal orientation, and grouped into diblocks, each containing 64 planes. The FD contains 14 diblocks, totalling 896 planes, whereas the ND contains 3 diblocks totalling 192 planes. However, the ND also consists of a Muon Catcher region, positioned right after the active region, consisting of 22 planes of the normal NOvA detector design, 2 modules high and 3 modules wide, sandwiched with 10 steel plates to help range out muons mainly from the ν_μ charge current interactions [4, 20].

Each cell is filled with a liquid scintillator consisting of mineral oil with a mixed in 4.1% pseudocumene as the scintillant [22]. Each cell contains a single wavelength shifting fibre with double the length of the cell, looping at one end and connecting to the readout at the other. As light travels through the fibre, it is attenuated by about a fraction of ten for the FD cells. The PVC walls of the detector cells are loaded with highly reflective titanium dioxide, with light typically bouncing off the PVC walls about 8 times before being captured by the fibre [20].

The total mass of the FD is about 14 kT and of the ND about 0.3 kT, with active volume, consisting of the liquid scintillator, making up about 70% of the total detector volume [20].

The NOvA detectors are specifically designed for electromagnetic shower identification, with radiation length of 38 cm, which amounts to ~ 7 planes for particles travelling perpendicular to the detector planes [4]. This is particularly useful to distinguish electrons and π^0 s.

COMMENT: *The MIP energy loss for electrons (similarly to muons) can be found with a similar method as used in the AbsCal_technote_1stAna in TestBeam (page 2).*

1.3 Data Acquisition

The signal from the wavelength shifting fibres is read out by an Avalanche Photodiode (APD), converting the scintillation light into electrical signal, with a high quantum efficiency of $\sim 85\%$ and a gain of 100 [20]. An example APD is shown on Fig. 1.5. Both ends of each fibre are connected to one of the 32 pixels on the APD, with each APD reading out signal from one module. To maximise the signal to noise ratio, the APDs are cooled to $-15\text{ }^{\circ}\text{C}$ by a thermoelectric cooler, with heat carried away by a water cooling system [20].

The combination of the APD quantum efficiency and the light yield, determined by the PVC reflectivity and scintillator and fibre response, result in a signal requirement of at least 20 photoelectrons in response to minimum ionizing radiation at the far end of the FD cell [20].

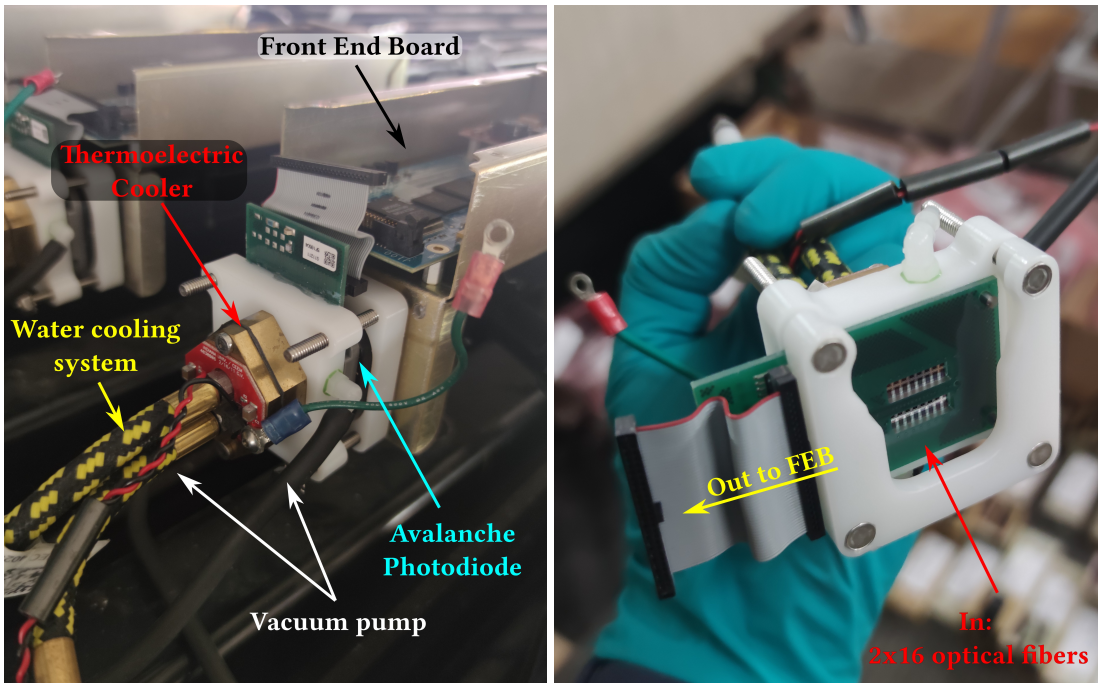


Figure 1.5: The modules with Avalanche Photo Diodes for NOvA mounted on top of the detector on the left picture, and shown from the bottom on the right. The individual components of the module are described. The left picture shows a disconnected ribbon cable and ground cable, which are normally connected to the front end board.

Each APD is connected to a single Front End Board (FEB), shown on Fig. 1.6, which amplifies and integrates the APD signal, determines its amplitude and arrival time, before passing it to the data acquisition system (DAQ). The APD signal is first passed to a custom NOvA Application-Specific Integrated Circuit (ASIC), which is

design to maximize the detector sensitivity to small signals. ASICs amplify, shape and combine the signal, before sending it to an Analog-to-Digital Converter (ADC). The combined noise from the APD and the amplifier is equivalent to about 4 photo-electrons, which, compared to an average photoelectron yield from the far end of the FD cell of 30, results in a good signal and noise separation [20]. The digitized data from an ADC is sent to a Field Programmable Gate Array (FPGA), which extracts the time and amplitude of the ADC signals, while subtracting noise based on a settable threshold. FPGAs employ multiple correlated sampling method to reduce noise and increase time resolution of the signal [23].

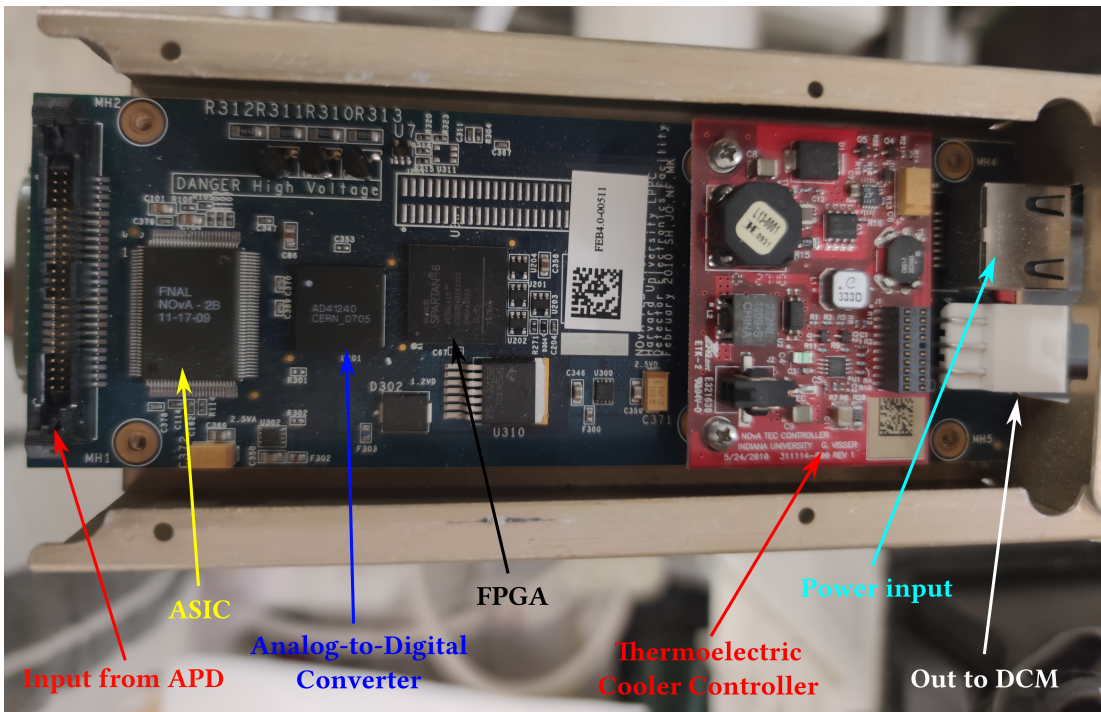


Figure 1.6: An example of a NOvA Front End Board with individual components labelled.

All of the NOvA front end electronic (APDs and FEBs) are operated in a continuous readout mode, without requiring any external triggers [20]. Due to higher detector activity during beam spills, the ND FEBs work in a higher frequency of 8 MHz, whereas the FD FEBs suffice with 2 MHz sampling frequency [23].

DAQ Software (what happens to the signal after the FEBs) is described in docdb:1233.
Not sure if this is the final design though.

Triggers

1.4 Data Processing and Event Reconstruction

Basic description of the process from raw data to final predictions (or just cafs?)

We are saving all the ADC and TDC (Time Digital Converter I believe) values to the RawDigit. Then they are fitting in the Calibrator to a functional form and converted to PE by fitting for the peak ADC.

Maybe talk about data quality as well? Good runs and so on...

Reconstruction - describe the reconstruction tools used to get the final products, focusing on the electron reconstruction.

Clustering into slices - how is that done?

Reconstruction of prongs and tracks. Electron showers

1.5 Simulation

1.5.1 Neutrino Beam Simulation

Should I mention that in the past we used Fluka, but now we're using Geant4

Package to Predict the FluX

Should I talk about this now or should I talk about the simulations (and their corrections) together?

I did this in the beginning of my thesis so maybe I should mention this. Especially the possible improvements and what I've done for them (enough to say I looked at it?)

Constraining the Hadron Production Systematic Uncertainty in NOvA

Again, should I discuss it here or somewhere else? Maybe not necessary as a full section. Not sure if I should include a discussion on nu-on-e, or low nu studies here, or just PPFX improvements.

1.5.2 Simulation of the Neutrino Interactions

NOvA Reweighting of the Neutrino Interaction Predictions

1.5.3 Simulation of the Detector Response

Should I join this with the other simulation subsection?

1.6 Detector Calibration

The purpose of calibration is to make sure that we get the same amount of energy wherever or whenever it's deposited in whichever of NOvA's detectors and to express this amount of energy in physical units. The NOvA calibration uses cosmic ray muons, which provide a consistent, abundant, and well-understood source of energy deposition.

Creating calibration samples

We want to select good quality cosmic ray muons. First, we remove beam related events based on their time stamps relative to the time of the beam spill. Next we apply reconstruction to get the CellHit, slicer, and track information, followed by a track-based selection to remove misreconstructed and poor quality events.

Since energy deposition depends on the path length particle travels through a cell, we only use hits for which we can reliably calculate their path length. We call these hits **tricell** hits, as we require that all accepted hits are accompanied by a recorded hit in both neighbouring cells of the same plane, as shown on Fig. 1.7. In case there is a bad channel in a neighbouring cell, we ignore this channel and look one cell further. We can then calculate the path length simply as the cell width divided by the cosine of the direction angle [? ?].

For the absolute calibration we select muons that stop inside the detector, by identifying muons with a Michel electron at the end of their track [?].

For each data period or epoch and for each version of the simulation we create two calibration samples that are used as the input for the relative and absolute calibration. The samples are called [?]

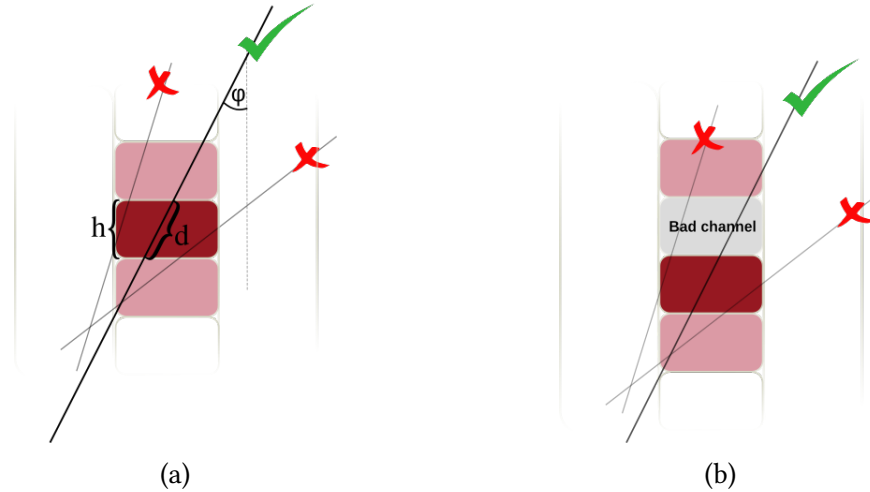


Figure 1.7: Illustration of the tricell condition (a). We only use hits that have two surrounding hits in the same plane to be used in the NOvA calibration. This is to ensure a good quality of the path length (d) reconstruction, which is calculated from the known cell height (h) and the reconstructed track angle (φ). In case the hit is next to a bad channel (b), we ignore this bad channel and require a hit in the next cell over.

- `pclist` = **list** of **pre-calibrated hist**; Contains all selected cosmic muon events and is used in the relative calibration;
- `pcliststop` = `pclist` files only containing stopping muons used for the absolute calibration

Fibre brightness

For data, the relative calibration is done for each individual cell in each plane to properly account for any potential variations, repeating the attenuation fit $N_{cell} \times N_{plane}$ times. However, generating enough simulated events turned out to be computationally expensive. Therefore, assuming the simulated detector is approximately uniform plane to plane, for simulation we can "consolidate" the detector planes and only consider variations in the two views. Therefore for simulation we would repeat the fit $N_{cell} \times N_{view}$ times [? ?].

However, there are some variations in the detector response cell by cell that can be caused by different fibre brightnesses, but also by different qualities of the scintillator, air bubbles, APD gains, looped or zipped fibres and potentially others. We want to include these variations in the simulation to better match data. To emulate these differences in the simulation without the need to simulate every cell individually, we divide each detector into 12 brightness bins, as shown on Fig. 1.8. These brightness

bins describe the relative differences in the detector response between individual cells [?]. Therefore in the end, for simulation we perform the attenuation fit $N_{cell} \times N_{view} \times N_{BrightnessBin}$ times.

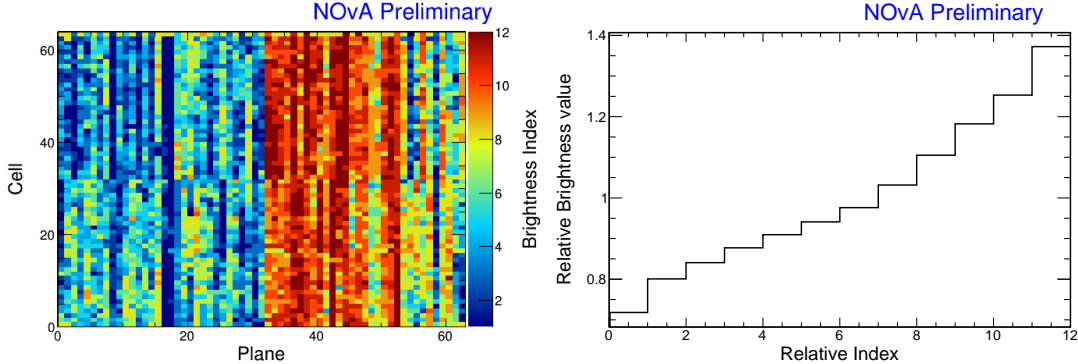


Figure 1.8: The Test Beam detector is (like the standard NOvA detectors) divided into 12 brightness bins (left plot), each representing a relative difference in energy response (right plot) due to different brightnesses of the fibres, scintillators, or readout.

To divide each detector into the 12 brightness bins, we use results from the relative calibration. Specifically we take the result of the attenuation fit (equal to the average response) in the centre of each cell to fill a 2D histogram. Then we normalize this histogram by dividing the response in each Cell \times View \times Plane by the average response in the corresponding Cell \times View. All uncalibrated cells get assigned the average response (1 in normalized histogram). Then we make a 1D histogram filled with the normalized responses of each cell and divide this histogram into 12 equally populated bins (so each bin represents approximately the same number of detector cells, shown on the left plot of Fig. 1.8). The mean normalized response in each bin represents the relative brightness value of this bin (right plot of Fig. 1.8).

TO DO: *Describe the absolute and relative calibration just in text* The NOvA calibration consists of two parts [?]:

1. The **relative calibration** corrects for attenuation of scintillator light as it travels through the cell to the readout, as well as for differences between detector cells. This correction is calculated for each cell separately.
2. Followed by the **absolute calibration**, which only uses stopping muons when they are minimum ionising particles. In the absolute calibration we calculate a scale between the measured energy deposition, corrected by the relative calibration, and the simulated energy deposition in physical units of MeV. This

scale is calculated for each time period and each detector separately, which ensures the energy deposition is directly comparable wherever or whenever it occurred.

TO DO: Just describe these units in text instead of here The basic units and variables used to define energy deposited in the NOvA detectors are listed in table 1.1.

| | |
|--------|---|
| ADC | The digitized charge collected by the APDs from the Analog to Digital Converter [?]. |
| PE | Number of Photo Electrons. Calculated by a simple rescaling of the best estimate of the peak ADC. The PE per ADC scale only depends on the FEB type and the APD gain settings. This conversion is done before the calibration and PE serves as the base unit for calibration. |
| PECorr | Corrected PE after applying the relative calibration results. The correction is a ratio between an average energy response (a pre-determined semi-arbitrary number) and the result of the the relative calibration fit (also called attenuation fit), which depends on w, cell, plane, epoch and detector. This makes the energy response equivalent across each detector. |
| MEU | Muon Energy Unit is the mean detector response to a stopping cosmic minimum ionising muon. For true variables it's equivalent to the mean MeV/cm and for reconstructed variables to the mean PECorr/cm. |
| MeV | Estimated energy deposited in the scintillator calculated from PECorr using the results of the absolute calibration. Additional correction for dead material needs to be made in order to get an estimate of the calorimetric energy. |

Table 1.1: Definitions of variables commonly used in calibration [? ?].

TO DO: Change this equation to be simpler and also include T/S corrections The final result of the NOvA calibration is the deposited energy in terms of physical units, which is in effect calculated as:

$$E_{dep}[\text{MeV}] = \underbrace{\frac{\text{MEU}_{truth}[\text{MeV}/\text{cm}]}{\text{MEU}_{reco}[\text{PECorr}/\text{cm}]}}_{\substack{\text{Absolute calibration} \\ (\text{Detector, epoch})}} \times \underbrace{\frac{\text{Average response}[\text{PECorr}]}{\text{Fitted response}[\text{PE}]}}_{\substack{\text{Relative calibration} \\ (\text{Detector, epoch, plane, cell, w})}} \times \underbrace{\left[\frac{\text{PE}}{\text{ADC}} \right]}_{\substack{\text{Scale} \\ (\text{APD Gain, FEB})}} \times \text{Signal}[\text{ADC}], \quad (1.1)$$

where both the relative calibration results (blue fraction) and the absolute calibration results (red fraction) are stored in a database and applied together with the ADC-to-

PE scale during processing of every hit in the NOvA detectors.

1.6.1 Threshold and shielding correction

Energy deposited far away from the readout may get attenuated enough to be shifted below the threshold. These low energy depositions would be missing from the attenuation fit, biasing it towards larger light levels with increasing distance from the readout. Similar effect, specifically for the vertical cells, is caused by using cosmic muons for calibration and applying it to beam muons. The top of the detector effectively shields the bottom, skewing the energy distribution of cosmic muons. To correct for both of these effect, we use the simulation plist sample to calculate the threshold and shielding (also called threshold and shadowing) correction by comparing the true and reconstructed information. We apply this correction before the attenuation fits [?].

1.6.2 Relative calibration

Relative calibration corrects for the attenuation of the scintillator light by fitting the average detector response over the position in each cell (w), separately for every cell inside each detector. Dividing the "average response" of the detector by the result of the attenuation fit for each Plane \times Cell $\times w$ combination effectively removes relative differences within and between all cells across the entire detector. The average response is a single constant number chosen to approximately represent the average response in the middle of the cell. Its value is for the far detector and Test Beam 39.91 PE/cm and for the near detector 37.51 PE/cm. The value of the average response has no impact of the calibration results, as the absolute scale of the detector response is determined during the absolute calibration and relative calibration only serves to remove the relative differences [? ?].

To create the attenuation fit we use the following procedure [?]:

1. Create the *attenuation profiles*. Attenuation profiles are essentially profile histograms of detector response in terms of PE/cm as a function of position in the cell (w) for each cell in all planes. We construct the attenuation profiles over a little wider range than the actual length of the cell and always with 100 bins for

each detector. This means that smaller detectors, like the Test Beam detector, have a finer binning ($\sim 3\text{cm/bin}$) compared to the Far Detector ($\sim 18\text{cm/bin}$).

2. Analyse the attenuation profiles. The job to create the attenuation profiles also creates validation histograms, which should be analysed prior to performing the attenuation fit to make sure the attenuation profiles look as expected.
3. Apply the threshold and shielding correction that was created before the relative calibration.
4. Do the attenuation fit over the full length of each cell. The fit consists of
 - (a) an exponential fit, which combines two cases. First, when the scintillating light travels the short distance straight to the readout, and second, when it goes to the far side of the cell and loops around before going to the readout. The fitted function has a form:

$$y = C + A \left(\exp \left(\frac{w}{X} \right) + \exp \left(-\frac{L+w}{X} \right) \right), \quad (1.2)$$

where y is the fitted response, L is the length of the cell and C , A and X are the fitted parameters. X also represents the attenuation length.

- (b) Smoothing of the residuals from the exponential fit, mainly at the end of cells, with the LOcally WEighted Scatter plot Smoothing (LOWESS) method.
5. Check the plots of the attenuation fit for a selection of cells.
6. Save the fit result to the database in the form of two csv tables. The `calib_atten_consts.csv` table holds the results of the exponential fit, together with the final χ^2 of the fit. The `calib_atten_points.csv` table holds the results of the LOWESS smoothing.

To ensure the quality of the attenuation fit, we only apply the results if the final $\chi^2 < 0.2$. If $\chi^2 > 0.2$, we ignore the results for this cell and mark it as *uncalibrated*.

1.6.3 Absolute calibration

To find the absolute energy scale, we apply the relative calibration results on the stopping muon sample and look at the energy they deposited in cells 1-2 meters from the end of their tracks. In this track window they are approximately minimum ionising particles and their energy deposition is almost constant and well understood. Additionally, we don't use hits from the edges of a cell, as those might be affected by the lower number of events, fibre endings, or loops.

For each calibrated data and simulation sample we take a mean of the corrected deposited energy distribution, separate for each view. We then take a simple average from the two views to get the final MEU_{reco} in units of PECorr/cm for each sample [?]. Additionally, from simulation we can get the mean of the distribution of the true deposited energy in the scintillator, $\text{MEU}_{\text{truth}}$ in units of MeV/cm for the same sample of stopping muons.

We ignore the energy that is lost in the dead material (PVC extrusions) and deal with it separately. The absolute energy scale for each sample is then the ratio of $\text{MEU}_{\text{truth}}/\text{MEU}_{\text{reco}}$. We save these absolute energy scales in another csv table called `calib_abs_consts.csv` which stores the MEU values and their errors.

As part of the absolute calibration we also produce validation plots that show the effect of calibration on the distribution of the stopping muons. We analyse these plots and if everything looks all right we load all the csv tables into the database.

1.7 Systematic Uncertainties at NOvA

1.7.1 Systematic Uncertainties Related to the NOvA Neutrino Beam

Hadron production and focusing systematic uncertainties

Principal component analysis

Maybe briefly also mention the POT scaling normalization uncertainty.

1.7.2 Systematic uncertainties for NOvA detectors

Neutrino interaction systematic uncertainties

Energy scale systematic uncertainty

Cell edge calibration systematic uncertainty

Detector ageing systematic uncertainty

Glossary

| | |
|------|---|
| CP | Charge conjugation Parity (symmetry) |
| NOvA | NuMI Off-axis ν_e Appearance (experiment) |
| NuMI | Neutrinos from the Main Injector |
| POT | Protons On Target |
| FHC | Forward Horn Current (neutrino mode) |
| RHC | Reverse Horn Current (antineutrino mode) |
| ND | Near Detector |
| FD | Far Detector |
| NDOS | Near Detector on the Surface |
| PVC | Polyvinyl chloride |
| APD | Avalanche Photodiode |
| FEB | Front End Board |
| DAQ | Data Acquisition |
| ASIC | Application-Specific Integrated Circuit |
| ADC | Analog-to-Digital Converter |
| FPGA | Field Programmable Gate Array |

Bibliography

- [1] Nova experiments official homepage. URL <https://novaexperiment.fnal.gov>. Cited February 2024.
- [2] Fermilab officail website homepage. URL <https://www.fnal.gov/>. Cited February 2024.
- [3] Gary Feldman for the NOvA Collaboration. Physics of the nova experiment. White paper, 2012. URL <https://nova-docdb.fnal.gov/cgi-bin>ShowDocument?docid=7733>. Public NOvA document: NOVA-doc-7733-v1, cited on 05.2020.
- [4] R.B. Patterson. The NOvA Experiment: Status and Outlook. *Nucl. Phys. B Proc. Suppl.*, 235-236:151–157, 2013. doi:[10.1016/j.nuclphysbps.2013.04.005](https://doi.org/10.1016/j.nuclphysbps.2013.04.005).
- [5] P. Adamson et al. First measurement of muon-neutrino disappearance in NOvA. *Phys. Rev. D*, 93(5):051104, 2016. doi:[10.1103/PhysRevD.93.051104](https://doi.org/10.1103/PhysRevD.93.051104).
- [6] M.A. Acero et al. First Measurement of Neutrino Oscillation Parameters using Neutrinos and Antineutrinos by NOvA. *Phys. Rev. Lett.*, 123(15):151803, 2019. doi:[10.1103/PhysRevLett.123.151803](https://doi.org/10.1103/PhysRevLett.123.151803).
- [7] M. A. Acero et al. Improved measurement of neutrino oscillation parameters by the NOvA experiment. *Phys. Rev. D*, 106(3):032004, 2022. doi:[10.1103/PhysRevD.106.032004](https://doi.org/10.1103/PhysRevD.106.032004).
- [8] M. A. Acero et al. Measurement of neutrino-induced neutral-current coherent π^0 production in the NOvA near detector. *Phys. Rev. D*, 102(1):012004, 2020. doi:[10.1103/PhysRevD.102.012004](https://doi.org/10.1103/PhysRevD.102.012004).
- [9] M. A. Acero et al. Measurement of the double-differential muon-neutrino charged-current inclusive cross section in the NOvA near detector. *Phys. Rev. D*, 107(5):052011, 2023. doi:[10.1103/PhysRevD.107.052011](https://doi.org/10.1103/PhysRevD.107.052011).
- [10] M. A. Acero et al. Measurement of the ν_e –Nucleus Charged-Current Double-Differential Cross Section at $\langle E_\nu \rangle = 2.4$ GeV using NOvA. *Phys. Rev. Lett.*, 130(5):051802, 2023. doi:[10.1103/PhysRevLett.130.051802](https://doi.org/10.1103/PhysRevLett.130.051802).

- [11] M. A. Acero et al. Measurement of ν_μ charged-current inclusive π^0 production in the NOvA near detector. *Phys. Rev. D*, 107(11):112008, 2023. doi:[10.1103/PhysRevD.107.112008](https://doi.org/10.1103/PhysRevD.107.112008).
- [12] P. Adamson et al. Search for active-sterile neutrino mixing using neutral-current interactions in NOvA. *Phys. Rev. D*, 96(7):072006, 2017. doi:[10.1103/PhysRevD.96.072006](https://doi.org/10.1103/PhysRevD.96.072006).
- [13] M. A. Acero et al. Search for Active-Sterile Antineutrino Mixing Using Neutral-Current Interactions with the NOvA Experiment. *Phys. Rev. Lett.*, 127(20):201801, 2021. doi:[10.1103/PhysRevLett.127.201801](https://doi.org/10.1103/PhysRevLett.127.201801).
- [14] M. A. Acero et al. Supernova neutrino detection in NOvA. *JCAP*, 10:014, 2020. doi:[10.1088/1475-7516/2020/10/014](https://doi.org/10.1088/1475-7516/2020/10/014).
- [15] M. A. Acero et al. Extended search for supernovalike neutrinos in NOvA coincident with LIGO/Virgo detections. *Phys. Rev. D*, 104(6):063024, 2021. doi:[10.1103/PhysRevD.104.063024](https://doi.org/10.1103/PhysRevD.104.063024).
- [16] M. A. Acero et al. Search for slow magnetic monopoles with the NOvA detector on the surface. *Phys. Rev. D*, 103(1):012007, 2021. doi:[10.1103/PhysRevD.103.012007](https://doi.org/10.1103/PhysRevD.103.012007).
- [17] P. Adamson et al. The NuMI Neutrino Beam. *Nucl. Instrum. Meth. A*, 806:279–306, 2016. doi:[10.1016/j.nima.2015.08.063](https://doi.org/10.1016/j.nima.2015.08.063).
- [18] Katsuya Yonehara. Megawatt upgrade of numi target system. 1 2022. URL <https://www.osti.gov/biblio/1844332>.
- [19] Leonidas Aliaga Soplin. *Neutrino Flux Prediction for the NuMI Beamline*. PhD thesis, William-Mary Coll., 2016.
- [20] D. S. Ayres et al. The nova technical design report. *NOvA Collaboration*, 2007. doi:[10.2172/935497](https://doi.org/10.2172/935497).
- [21] Yury Kudenko. Neutrino detectors for oscillation experiments. *JINST*, 12(06):C06003, 2017. doi:[10.1088/1748-0221/12/06/C06003](https://doi.org/10.1088/1748-0221/12/06/C06003).

- [22] S. Mufson et al. Liquid scintillator production for the NOvA experiment. *Nucl. Instrum. Meth. A*, 799:1–9, 2015. doi:[10.1016/j.nima.2015.07.026](https://doi.org/10.1016/j.nima.2015.07.026).
- [23] Xinchun Tian. NOvA Data Acquisition Software System. In *Meeting of the APS Division of Particles and Fields*, 9 2011.